

A low-rank tensor method to reconstruct sparse initial states for PDEs with Isogeometric Analysis

Alexandra Bünger* and Martin Stoll†

Abstract. When working with PDEs the reconstruction of a previous state often proves difficult. Good prior knowledge and fast computational methods are crucial to build a working reconstruction. We want to identify the heat sources on a three dimensional domain from later measurements under the assumption of small, distinct sources, such as hot chippings from a milling tool. This leads us to the need for a Prior reflecting this a priori information. Sparsity-inducing hyperpriors have proven useful for similar problems with sparse signal or image reconstruction. We combine the method of using a hierarchical Bayesian model with gamma hyperpriors to promote sparsity with low-rank computations for PDE systems in tensor train format.

Key words. Isogeometric Analysis, low rank decompositions, tensor train format, Bayesian inverse problem, sparse reconstruction

AMS subject classifications. 65F10, 65F50, 15A69, 35R30

1. Motivation. The reconstruction of sparse sources from noisy observation of a PDE model plays a significant role in many applications, varying from identifying heat sources [20] to finding the origin of a tumor growth [31]. Incorporating prior information about the sparsity of an unknown source into its recovery from noisy data arose as long as 40 years ago with first successful applications in geophysics, astrophysics, and ultrasonic imaging [9].

The general idea of using ℓ_p Tikhonov regularization techniques has since become highly popular to promote sparsity and has been extensively researched (cf. [13, 18] and references therein), mainly focusing on $1 \leq p \leq 2$ due to their global convexity properties. It has been shown that an ℓ_1 penalty can provide accurate sparse reconstructions [6] or even the sparsest possible solution under some additional assumptions [10]. Stronger sparsity promotion with $p < 1$ comes at the expense of global convexity and is therefore still an active research topic [32].

In the Bayesian framework, sparsity promotion can be efficiently modeled by considering a component-wise Gaussian prior model where the variances themselves are modeled as random variables underlying a sparsity promoting *hyperprior* model [5]. In this paper we will examine the application of a hybrid method using such hypermodels with gamma hyperpriors presented in [4]. The algorithm strongly promotes sparsity while retaining global convergence by switching between two models where the first is globally convex to drive the solution close to a unique minimizer and the other is more greedy towards stronger sparsity while suffering from local minima.

Let us assume a PDE model with Dirichlet boundary conditions on a 2D or 3D domain

*Technische Universität Chemnitz, Department of Mathematics, Chair of Scientific Computing, 09107 Chemnitz, Germany, alexandra.buenger@mathematik.tu-chemnitz.de

†Technische Universität Chemnitz, Department of Mathematics, Chair of Scientific Computing, 09107 Chemnitz, Germany, martin.stoll@mathematik.tu-chemnitz.de

Ω as

$$(1.1) \quad \frac{\partial}{\partial t} y(x, t) = \mathcal{L}y(x, t) \quad \text{on } \Omega \times (0, T],$$

$$(1.2) \quad y(x, t = 0) = u_0(x) \quad \text{on } \Omega \times 0,$$

$$(1.3) \quad y(x, t) = y_0(x) \quad \text{on } \partial\Omega \times (0, T],$$

with a PDE operator \mathcal{L} such as $\mathcal{L}y(x, t) = \Delta y(x, t)$ for heat conduction. Here, $y(x, t)$ is the state at time t and $u_0(x, t)$ the respective initial state at time $t = 0$. Both are time-dependent functions on the domain Ω and time-frame $(0, T]$ with end time T .

We consider being given a noisy observation at the end time T stemming from the evolution via the PDE model (1.1)–(1.3),

$$(1.4) \quad z(x) = y(x, T) + e.$$

Our goal is to recover the initial state under the presence of additive noise e , e.g., measurement errors, and the prior assumption of u_0 being sparse.

In this paper, we will study a Bayesian approach to the problem of reconstructing u_0 under the assumption of Gaussian additive noise and a sparsity inducing prior formulation. We make use of the methods developed in [4] and tailor them to our model in section 2. The original algorithm requires a large number of matrix-vector multiplications with the parameter-to-observable map, which in our case includes a complete solution of the governing PDE and thus can be infeasibly large and dense.

The PDE model can be discretized in space and time into a linear equation system using some time-stepping method and a Galerkin type discretization, which we will introduce in section 3. We introduce the space discretization using an Isogeometric Analysis (IGA) scheme in subsection 3.1 and the full space-time discretization in subsection 3.2. As the resulting discretization would be large and dense, we propose a low-rank approximation method for the IGA discretization in section 4 and a suitable solver tailored to working with low-rank tensor structured data in section 5 to perform matrix-vector multiplications or solving the arising KKT system without computing the matrices directly. The resulting numerical scheme profits from small storage requirements and robustness allowing to compute even very large-scale problems, which would prove infeasible with traditional methods. In section 6 we provide numerical examples with an exemplary 2D problem and 3D models to show the effectiveness and robustness of the resulting method comparing different hyperprior setups.

2. Sparsity inducing hyper prior. We will first briefly review the method for sparsity inducing hyperpriors as the local hybrid IAS (iterative alternating sequential) algorithm introduced in [4] and later extended in [3] from a Bayesian point of view.

We consider the linear observation model with additive Gaussian noise resulting from the PDE problem with uncertain initial values u_0 ,

$$(2.1) \quad z = Au_0 + e, \quad e \sim \mathcal{N}(0, \Sigma),$$

where $A \in \mathbb{R}^{n \times m}$ is the parameter-to-observable map, which transfers the uncertain inputs u_0 to the observable outputs y , and $\Sigma \in \mathbb{R}^{m \times m}$ is a symmetric positive semidefinite covariance

matrix. Without loss of generality, we assume the noise to be white, i.e. $\Sigma = I$. This gives the likelihood probability density function (pdf)

$$(2.2) \quad \pi_{z|u_0}(z|u_0) \propto \exp\left(-\frac{1}{2}\|Au_0 - z\|^2\right).$$

We believe the unknown u_0 to be sparse. To incorporate this into the prior model, we consider a component-wise Gaussian prior model,

$$(2.3) \quad u_0 \sim \mathcal{N}(0, D_\theta), \quad D_\theta = \text{diag}(\theta_1, \dots, \theta_n) \in \mathbb{R}^{n \times n},$$

where the variances θ are not known. Thus, θ itself are random variables where smaller variances promote values closer to zero. The a priori belief about θ is thus incorporated into a *hyperprior* pdf $\pi_\theta(\theta)$ leading to a hierarchical prior model. The conditional prior density of u_0 with given θ now has the form

$$(2.4) \quad \pi_{u_0|\theta}(u_0|\theta) \propto \frac{1}{\prod_{j=1}^n \sqrt{\theta_j}} \exp\left(-\frac{1}{2}\|D_\theta^{-1/2}u_0\|^2\right) = \exp\left(-\frac{1}{2}\|D_\theta^{-1/2}u_0\|^2 - \frac{1}{2}\sum_{j=1}^n \log \theta_j\right).$$

Now we need to estimate θ as well as u_0 and chose an appropriate prior density for its representation. One class of hyperpriors π_θ to promote the sparsity of our solution is that of generalized gamma distributions,

$$(2.5) \quad \pi_\theta(\theta) = \pi_\theta(\theta|r, \beta, \vartheta) = \frac{|r|^n}{\Gamma(\beta)^n} \prod_{j=1}^n \frac{1}{\vartheta_j} \left(\frac{\theta_j}{\vartheta_j}\right)^{r\beta-1} \exp\left(-\left(\frac{\theta_j}{\vartheta_j}\right)^r\right),$$

with $r \in \mathbb{R} \setminus \{0\}, \beta > 0, \vartheta > 0$. This family of priors allows large outliers in θ while overall favoring small values [4].

With this we not only estimate x_0 but θ as well, based on their joint posterior distribution,

$$(2.6) \quad \pi_{u_0, \theta}(u_0, \theta|y) \propto \pi_{u_0|\theta}(u_0|\theta) \pi_\theta(\theta) \pi_{z|u_0}(z|u_0).$$

To find a suitable sparse reconstruction for u_0 , we need to compute the maximum a posteriori (MAP) estimate, which is the minimizer of the negative logarithm of the posterior pdf (2.6),

$$(2.7) \quad (u_0^*, \theta^*) = \arg \min_{u_0, \theta} \mathcal{F}(u_0, \theta|r, \beta, \vartheta)$$

$$(2.8) \quad = \arg \min_{u_0, \theta} \frac{1}{2}\|z - Au_0\|^2 + \frac{1}{2}\sum_{j=1}^n \frac{u_{0,j}^2}{\theta_j} - \left(r\beta - \frac{3}{2}\right) \sum_{j=1}^n \log \frac{\theta_j}{\vartheta_j} + \sum_{j=1}^n \left(\frac{\theta_j}{\vartheta_j}\right)^r.$$

Note that the objective function $\mathcal{F}(u_0, \theta)$ consists of four terms of which one depends on u_0 only, two depend only on θ and one is dependent on both variables. This gives rise to an hybrid algorithm alternating between updates of u_0 and θ .

The authors of [4] suggest using an Iterative Alternating Sequential algorithm (IAS) for this computation. Here, each iteration consists of two updates,

$$(2.9) \quad u^i, \theta^i \rightarrow u^{i+1} \rightarrow \theta_{i+1},$$

where we first fix θ to update u^{i+1} and afterwards fix u^{i+1} to update θ ,

$$(2.10) \quad u^{i+1} = \arg \min_u \{\mathcal{F}(u, \theta^i)\}, \theta^{i+1} = \arg \min_\theta \{\mathcal{F}(u^{i+1}, \theta)\}.$$

Both minimizations have an exact condition for the minimizer and are relatively simple to compute. The update of u results in the solution of a quadratic minimization problem, i.e.,

$$(2.11) \quad u^{i+1} = \arg \min_u \|Au - z\|^2 + \|D_\theta^{-1/2}u\|^2.$$

To approximate the solution, we can solve (2.11) as it is or solve a reduced least squares problem. For this we introduce a change of variables as $w = D_\theta^{-1/2}u$ and find the least squares solution of

$$(2.12) \quad AD_\theta^{1/2}w = z.$$

This can be easily solved, e.g. by a CGLS (Conjugate Gradient Least Squares) algorithm, as suggested in [3]. We will later discuss the structure of A for our PDE model and propose a low rank method to efficiently solve this minimization problem.

To then update θ we can compute its components θ_j independently from each other. For each component the first order optimality conditions applied to (2.8) read

$$(2.13) \quad 0 = \frac{\partial \mathcal{F}}{\partial \theta_j} = -\frac{1}{2} \frac{u_j^2}{\theta_j^2} - \left(r\beta - \frac{3}{2}\right) \frac{1}{\theta_j} + r \frac{\theta_j^{r-1}}{\vartheta_j^r}.$$

To numerically solve this equation, [4] suggests the change of variables $\theta_j = \vartheta_j \xi_j$, $u_j = \sqrt{\vartheta_j} z_j$. Then, we can write $\xi_j = \varphi(|z_j|)$ and we get the initial value problem

$$(2.14) \quad \varphi'(z) = \frac{2z\varphi(z)}{2r^2\varphi(z)^{r+1} + z^2}, \quad \varphi(0) = \left(\frac{\eta}{r}\right)^{1/r}.$$

From this the update for θ_j can be computed with some numerical time integrator.

Alternating between updating u and updating θ gives rise to the standard IAS algorithm.

2.1. Hyperprior parameters and hierarchical IAS algorithm. The effectiveness of the alternating scheme depends highly on the choice of parameters for the hyperprior, r , β and ϑ . A detailed analysis of these parameters is available in [4], which we want to summarize now. We additionally analyze the choice of parameters in our numerical experiments in Section 6.

The choice of r and β affects the sparsity of the solution and determines the convexity of the objective function while ϑ can be seen as a sensitivity scaling where $\vartheta_j = \frac{C}{\|Ae_j\|^2}$ with some constant $C > 0$ (cf. [3]). The constant C should depend on the signal-to-noise ratio (SNR).

Calvetti et al. propose two modifications to the general IAS algorithm to update the hypermodel component-wise and ensure convexity. When $r > 1$ and β follows $r\beta > 3/2$ the objective function is globally convex. Additionally, the objective function is convex for $0 < r < 1$, $r\beta > 3/2$ or $r < 0$ and $\beta > 0$ when $\theta_j < \vartheta_j \left(\frac{\eta}{r|r-1|}\right)$. This can be exploited by

choosing two hypermodels M_1 and M_2 , where M_1 satisfies the global convexity conditions and M_2 is the desired sparsity promoting model.

Global hybrid IAS. The first method proposed starts the iteration with model M_1 and carries out a switch to model M_2 for all parameters at once after a certain number of iterations. The first iterations drive the objective function towards the global minimum and afterwards we trade global convexity for stronger sparsity promotion. The algorithm is outlined in [Algorithm 2.1](#).

Local hybrid IAS. The second proposition starts with model M_2 as well but updates the models locally by switching individual components of θ_j to the other model M_2 when θ_j is below the threshold for convexity. To ensure preservation of convexity an additional bound constraint is applied to components, which were switched to model M_2 . [Algorithm 2.2](#) illustrates the iteration for this method.

We will consider both methods in our experiments for a gamma ($r = 0.5$) and inverse gamma ($r = -1$) hyperprior model.

Algorithm 2.1 Global hybrid IAS

- 1: Input: noisy z , parameter-to-observable map A , noise covariance matrix Σ , hypermodel M_1 with $(r_1, \beta_1, \vartheta_1)$, hypermodel M_2 with $(r_2, \beta_2, \vartheta_2)$, switch point $i_s > 0$,
 - 2: Set $\theta_0 = \vartheta_1$
 - 3: **for** $i = 1, \dots, \text{maxIter}$ or until convergence **do**
 - 4: Solve $\min_{u_i} \|Au_i - z\|^2 + \|D_\theta^{-1/2}u_i\|^2$
 - 5: **if** $i < i_s$ **then**
 - 6: Update θ with u_i and parameters from M_1
 - 7: **else**
 - 8: Update θ with u_i and parameters from M_2
 - 9: **end if**
 - 10: **end for**
 - 11: Output: estimated initial values $u_0 = u_i$ and variance θ
-

3. Space-time discretization of A . To use the method described in [section 2](#) we need a representation of the parameter-to-observable map A . For our PDE model [\(1.1\)–\(1.3\)](#), we need an appropriate discretization to build this mapping. We will now introduce Isogeometric Analysis for the space discretization in [subsection 3.1](#) and the time-discretization with an implicit Euler scheme in [subsection 3.2](#).

For the space discretization a Finite Element Method (FEM) [\[11\]](#) is the most prominently used choice and has seen a wide range of applications in both engineering and science [\[27\]](#). But recently a new approach called Isogeometric Analysis (IGA) [\[7\]](#) has gained popularity. This approach arose from the desire to integrate numerical analysis directly into CAD (computer aided design) tools [\[7\]](#). It abolishes the need for time consuming meshing steps and preprocessing needed in classical Finite Element Analysis [\[1\]](#) in addition to working on exact geometric representations instead of an approximation.

Furthermore, this method admits a tensor-product based structure which gives rise to a very effective low-rank method developed in [\[22\]](#) and refined in [\[21, 28\]](#). This has been shown

Algorithm 2.2 Local hybrid IAS

-
- 1: Input: noisy z , parameter-to-observable map A , noise covariance matrix Σ , hypermodel M_1 with $(r_1, \beta_1, \vartheta_1)$, hypermodel M_2 with $(r_2, \beta_2, \vartheta_2)$
 - 2: Set $\theta_0 = \vartheta_1$, $I = \emptyset$
 - 3: **for** $i = 1, \dots, \text{maxIter}$ or until convergence **do**
 - 4: Solve $\min_{u_i} \|Au_i - z\|^2 + \|D_\theta^{-1/2}u_i\|^2$
 - 5: Apply bound constraint to $u_{i,j}$ with $j \in I$
 - 6: **for** $j = 1, \dots, n$ **do**
 - 7: **if** $\theta_j \geq \vartheta_j(\frac{\eta}{r|r-1|})$ **then**
 - 8: update θ_j with model M_1
 - 9: **else**
 - 10: update θ_j with model M_2
 - 11: $i = I \cup \{j\}$
 - 12: **end if**
 - 13: **end for**
 - 14: **end for**
 - 15: Output: estimated initial values $u_0 = u_i$ and variance θ
-

to be very efficient in combination with tensor train calculations [24] in our recent work on PDE-constrained optimal control problems [2].

3.1. Isogeometric Analysis discretization. Isogeometric Analysis benefits from the use of high order spline functions, such as B-splines and NURBS, as their basis. A geometric domain is represented exactly using a set of such splines, which are subsequently used to build a solution space for solving a PDE problem [17]. In this paper we will focus on the use of B-splines but note that a generalization to other popular spline spaces, such as NURBS (Non-uniform rational B-splines) [26, 12], is possible. The notation and derivation in this section as well as section 4 follow our work in [2].

A set of n B-splines is uniquely defined by choosing a vector $\xi = \{\hat{x}_1, \dots, \hat{x}_{n+p+1}\}$, called the open knot vector, with

$$(3.1) \quad 0 = \hat{x}_1 = \dots = \hat{x}_{p+1} < \hat{x}_{p+2} \leq \dots \leq \hat{x}_n < \hat{x}_{n+1} = \dots = \hat{x}_{n+p+1} = 1,$$

and a degree p , where the first and last knot are repeated $p + 1$ times and for all other knots duplicate knots are allowed up to multiplicity p . The parameter n determines the number of resulting B-splines $\beta_{i,p}$ with $i = 1, \dots, n$.

For each knot vector ξ as in (3.1), the according B-splines $\beta_{i,p}$ of degree p with $i = 1, \dots, n$ are uniquely defined by the recursion

$$(3.2) \quad \beta_{i,0}(\hat{x}) = \begin{cases} 1 & \text{if } \hat{x}_i \leq \hat{x} < \hat{x}_{i+1}, \\ 0 & \text{otherwise,} \end{cases}$$

$$(3.3) \quad \beta_{i,j}(\hat{x}) = \frac{\hat{x} - \hat{x}_i}{\hat{x}_{i+j} - \hat{x}_i} \beta_{i,j-1}(\hat{x}) + \frac{\hat{x}_{i+j+1} - \hat{x}}{\hat{x}_{i+j+1} - \hat{x}_{i+1}} \beta_{i+1,j-1}(\hat{x}),$$

where $j = 1, 2, \dots, p$ and $i = 1, \dots, n$. Each resulting B-spline $\beta_{i,p}$ has the local support $[\hat{x}_i, \hat{x}_{i+p+1}]$, see Figure 1 for an example. We use \mathbb{S}_ξ^p to denote the spline space spanned by the B-splines with degree p and knot vector ξ ,

$$(3.4) \quad \mathbb{S}_\xi^p = \text{span}\{\beta_{1,p}, \dots, \beta_{n,p}\}.$$

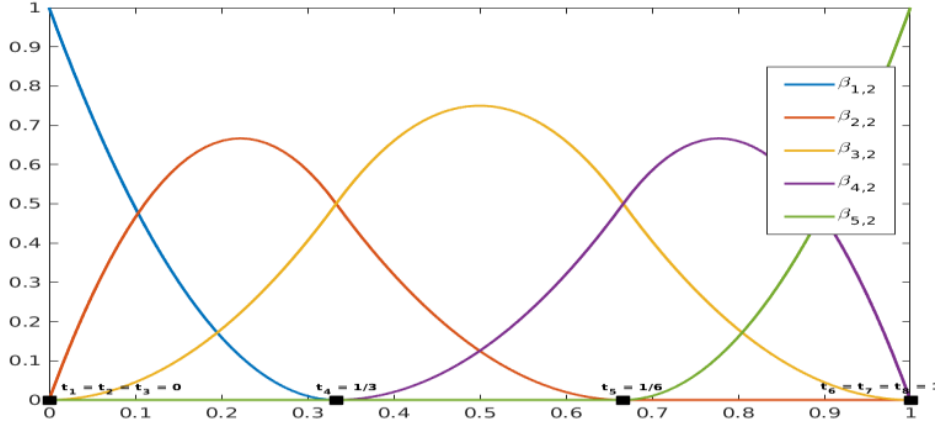


Figure 1: B-spline space with degree $p = 2$ and knot vector $\xi = [0, 0, 1/3, 1/2, 2/3, 1, 1]$.

To construct a space of D -dimensional basis functions \mathbb{S}^D , for $d = 1, \dots, D$ we define one-dimensional spline spaces $\mathbb{S}_{\xi_d}^{p_d}$ and vector valued functions $B^{(d)}(\hat{x}^{(d)})$, as the vectors holding all basis functions of dimension d ,

$$(3.5) \quad B^{(d)}(\hat{x}^{(d)}) = [\beta_1^{(d)}(\hat{x}^{(d)}), \dots, \beta_{n_d}^{(d)}(\hat{x}^{(d)})],$$

with one-dimensional variables $\hat{x}^{(d)}$.

We combine these spline spaces via tensor product to get a D -dimensional spline space $\mathbb{S}^D = \mathbb{S}_{\xi_1}^{p_1} \otimes \dots \otimes \mathbb{S}_{\xi_D}^{p_D}$ with an order D tensor of size (n_1, \dots, n_D) collecting all basis functions as

$$(3.6) \quad B(\hat{x}) = \bigotimes_{d=1}^D B^{(d)}(\hat{x}^{(d)}).$$

The tensor in (3.6) then is a function $B(\hat{x}) : \mathbb{R}^D \rightarrow \mathbb{R}^{n_1 \times \dots \times n_D}$ with variables $\hat{x} = (\hat{x}^{(1)}, \dots, \hat{x}^{(D)})^T$ and its elements are the D -dimensional basis functions

$$(3.7) \quad \beta_{\mathbf{i}}(\hat{x}) = \prod_{d=1}^D \beta_{i_d}^{(d)}(\hat{x}^{(d)}),$$

with multi-index $\mathbf{i} \in I = \{(i_1, \dots, i_D) \mid i_d = 1, \dots, n_d, d = 1, \dots, D\}$.

Given such a basis \mathbb{S}^D , we define a B-spline geometry mapping $G : \hat{\Omega} \rightarrow \Omega$ from the D -dimensional unit cube $\hat{\Omega} := [0, 1]^D$ onto an arbitrary geometric shape $\Omega \subset \mathbb{R}^D$ as

$$(3.8) \quad G(\hat{x}) = \sum_{\mathbf{i} \in I} C_{\mathbf{i}} \beta_{\mathbf{i}}(\hat{x}) = C : B(\hat{x}),$$

with control points $C_{\mathbf{i}} \in \mathbb{R}^D$. Here $C : B(\hat{x})$ denotes the Frobenius product of the two tensors, $C \in \mathbb{R}^{D \times n_1 \times \dots \times n_D}$ holding all the control points and B from (3.6).

Now that we have a spline representation of the geometry Ω , we use the same splines to construct discrete functions $u_h \in V_h \subset H^1(\Omega)$ as approximations to the solutions $u \in H^1(\Omega)$ of the PDE problem in (1.1)–(1.3).

The isogeometric solution space V_h is built as

$$(3.9) \quad V_h = \text{span}\{\beta_{\mathbf{i}} \circ G^{-1} : \mathbf{i} \in I\},$$

with an index set I such that $\beta_{\mathbf{i}}$ are the elements of \mathbb{S}^D . The functions in V_h are linear combinations of the basis functions with coefficients $u_{\mathbf{i}}$,

$$(3.10) \quad u_h = \sum_{\mathbf{i} \in I} u_{\mathbf{i}} (\beta_{\mathbf{i}} \circ G^{-1}).$$

We use this space for the spatial Galerkin discretization of the PDE system (1.1)–(1.3). Exemplary, for the boundary value problem $u(x) = f(x)$ in Ω , the weak formulation results in the bilinear form

$$(3.11) \quad a_m(u, v) = \langle u, v \rangle_2 = \int_{\Omega} uv \, dx,$$

called the mass term. Discretization with (3.9) results in the discrete mass term

$$(3.12) \quad a_{m,h}(u_h, v_h) = \int_{\Omega} u_h(x) v_h(x) \, dx = \int_{\hat{\Omega}} \sum_{\mathbf{i} \in I} u_{\mathbf{i}} \beta_{\mathbf{i}}(\hat{x}) \sum_{\mathbf{j} \in I} v_{\mathbf{j}} \beta_{\mathbf{j}}(\hat{x}) \omega(\hat{x}) \, d\hat{x},$$

with $\omega(\hat{x}) = |\det \nabla G(\hat{x})|$. The basis functions $\beta_{\mathbf{j}}$ are linearly independent. Thus, similarly to FEM, we can rewrite the bilinear forms as a matrix-vector product Au with vectorization of the coefficient set $u_{\mathbf{i}}$, $\mathbf{i} \in \mathcal{I}$, where A is realized as a mass matrix M with elements

$$(3.13) \quad M_{\mathbf{i},\mathbf{j}} = \int_{\hat{\Omega}} \beta_{\mathbf{i}} \beta_{\mathbf{j}} \omega \, d\hat{x}.$$

The same strategy is applied to any PDE operator $\mathcal{L}u(x)$, e.g. $\mathcal{L}u(x) = -\Delta u(x)$ results in the stiffness term

$$(3.14) \quad a_s(u, v) = - \int_{\Omega} (\Delta u) v \, dx = \int_{\Omega} \nabla u \cdot \nabla v \, dx,$$

$$(3.15) \quad a_{s,h}(u_h, v_h) = \int_{\Omega} (\nabla u_h(x)) \cdot \nabla v_h(x) \, dx = \int_{\hat{\Omega}} (Q(\hat{x}) \sum_{\mathbf{i} \in I} u_{\mathbf{i}} \nabla \beta_{\mathbf{i}}(\hat{x})) \cdot \sum_{\mathbf{j} \in I} v_{\mathbf{j}} \nabla \beta_{\mathbf{j}}(\hat{x}) \, d\hat{x},$$

with $Q(\hat{x}) = (\nabla G(\hat{x})^T \nabla G(\hat{x}))^{-1} |\det \nabla G(\hat{x})|$ (cf. [22]) resulting in the stiffness matrix K with elements

$$(3.16) \quad K_{\mathbf{i}, \mathbf{j}} = \int_{\hat{\Omega}} (Q \nabla \beta_{\mathbf{i}}) \cdot \nabla \beta_{\mathbf{j}} \, d\hat{x} = \sum_{k, l=1}^D \int_{\hat{\Omega}} q_{k, l} \frac{\partial}{\partial \hat{x}_l} \beta_{\mathbf{i}} \frac{\partial}{\partial \hat{x}_k} \beta_{\mathbf{j}} \, d\hat{x}.$$

With these matrices we can now discretize the parameter-to-observable map A in a general way before introducing additional low-rank approximations for M and K exploiting the underlying tensor product structure of the basis functions to reduce the computational effort and storage requirements of our problem. This low-rank approach has been successfully applied before to an optimal control problem in [2].

3.2. Discrete parameter-to-observable map. Considering the PDE problem given in (1.1) – (1.3), we now have a space discretization, which we need to combine with a suitable method for time discretization. For this time-stepping method we choose an implicit Euler scheme [23] and N_t equidistant time steps of length τ to discretize the time frame $t \in (0, T]$ into steps $t_i = i\tau$ for $i = 1, \dots, N_t$. With this we get the fully discrete system

$$(3.17) \quad \frac{My_i - My_{i-1}}{\tau} = -Ky_i, \quad \text{for } i = 2, \dots, N_t$$

$$(3.18) \quad My_1 = -\tau Ky_1 + Mu_0$$

$$(3.19) \quad z = Cy_{N_t} + e.$$

Here, y_i is the vector of B-spline coefficients for the discretization of the function $y(t_i)$ and C denotes the observation operator (e.g. an identity for a full observation at N_t). We will denote the vectors collecting all time steps as e.g. $\mathbf{y} = [y_1, \dots, y_{N_t}]^T$.

We can write this system of equations as one large equation system,

$$(3.20) \quad \underbrace{\begin{bmatrix} \tau K + M & & & \\ -M & \tau K + M & & \\ & \ddots & \ddots & \\ & & -M & \tau K + M \end{bmatrix}}_{\mathbf{K}} \begin{bmatrix} y_1 \\ \vdots \\ y_{N_t} \end{bmatrix} = \underbrace{\begin{bmatrix} M \\ 0 \\ \vdots \\ 0 \end{bmatrix}}_{\mathbf{M}_0} u_0,$$

$$(3.21) \quad z = \underbrace{\begin{bmatrix} 0 & \cdots & 0 & C \end{bmatrix}}_{\mathbf{C}} \begin{bmatrix} y_1 \\ \vdots \\ y_{N_t} \end{bmatrix} + e.$$

Using this formulation we can denote the equation from u_0 to z , the parameter-to-observable map A , as

$$(3.22) \quad z = Au_0 := \mathbf{CK}^{-1}\mathbf{M}_0 u_0.$$

This matrix A typically is dense and large, and even storing the full representation of \mathbf{K} may pose difficulties. Thus, computing A explicitly is usually infeasible. We will present a scheme to efficiently compute matrix-vector products with A without forming any full matrices. For

this, let us observe the structure of the arising matrices. We can also expressed them with the following Kronecker products,

$$(3.23) \quad \mathbf{C} = \begin{bmatrix} 0 & \cdots & 0 & 1 \end{bmatrix} \otimes C,$$

$$(3.24) \quad \mathbf{K} = \tau I_{N_t} \otimes K + II \otimes M,$$

$$(3.25) \quad \mathbf{M}_0 = \begin{bmatrix} 1 & 0 & \cdots & 0 \end{bmatrix}^T \otimes M,$$

where I_{N_t} is the $N_t \times N_t$ identity, II is a bidiagonal matrix with 1 on the diagonal and -1 on its first subdiagonal¹.

Note that here II results from the implicit Euler scheme. This scheme can be replaced by a different time stepping method like a Crank-Nicolson scheme [19] or others in which case II and the identity I_{N_t} will become different block matrices. Using a different time-stepping method would thus still maintain the general Kronecker product structure of the equations and be applicable for the following steps.

Now that we know the structure of our parameter-to-observable map we can take a closer look at solving the minimization problem in (2.11). In [4], the authors suggest using a CGLS method [14]. This method is most suited if the underlying matrix A is sparse and can be precomputed (cf. [29]) as it requires a large number of matrix-vector products with A and A^T .

Unfortunately, in the case of the PDE solution (3.22) the resulting matrix will most likely be dense and potentially very large. Thus, constructing A in full may not be feasible. In the following chapter we propose a low rank method that can be used to either calculate the matrix-vector products needed for CGLS in a compact and efficient way without assembly of A , or to solve the optimization problem (2.11) by rearranging it into a constrained minimization problem.

Substituting Au_0 in (2.11) by $\mathbf{C}y$ and using the PDE as a constraint leads to

$$(3.26) \quad \min_{u_0} \|\mathbf{C}y - z\|^2 + \|D_\theta^{-1/2}u_0\|^2$$

$$(3.27) \quad \text{s.t. } \mathbf{K}y = \mathbf{M}_0u_0.$$

Formulating its first order optimality conditions gives us the large scale saddle point system,

$$(3.28) \quad \begin{bmatrix} \mathbf{C}^T M \mathbf{C} & 0 & -\mathbf{K}^T \\ 0 & D_\theta^{-1/2} M D_\theta^{-1/2} & \mathbf{M}_0^T \\ -\mathbf{K} & \mathbf{M}_0 & 0 \end{bmatrix} \begin{bmatrix} y \\ u_0 \\ \lambda \end{bmatrix} = \begin{bmatrix} \mathbf{M}_0 \\ 0 \\ 0 \end{bmatrix}.$$

This type of system has been extensively researched and can generally be solved with e.g. preconditioned iterative methods (cf. [25]) or variational formulations [15]. But due to its potential size we will focus on a low rank method exploiting the underlying structure of the system. Here, each block has a Kronecker product structure as described in (3.23), which can be exploited efficiently by a low rank in time method presented in [30]. To further reduce the computational complexity we will now take a look back at the structure of the matrices M and K and outline how we can solve the resulting Kronecker product based system with a low rank tensor train method.

¹Syntax for MATLAB: $II = \text{spdiags}([-ones(N_t, 1), ones(N_t, 1)], -1 : 0, N_t, N_t)$;

4. Low Rank IGA. We see that the time discretization in (3.23)–(3.25) leads to a tensor product structure in the parameter-to-observable map. Using the method presented in [2] we can additionally approximate M and K as similar tensor products and exploit the resulting structure with low rank tensor train calculations. This exploit can either be utilized for the matrix-vector products in the CGLS scheme or to solve the saddle point system (3.28).

During the derivation of the mass and stiffness matrices, we did not pay attention to the tensor product structure of \mathbb{S}^D . We can either arrange M and K as matrices or as tensors of size $(\mathbf{n}, \mathbf{n}) = (n_1, \dots, n_D, n_1, \dots, n_D)$. With this tensor notation the mass and stiffness matrices in a multi-dimensional setting are represented in a compact way. We can write the mass term as a tensor M

$$(4.1) \quad M = \int_{\hat{\Omega}} \omega B \otimes B \, d\hat{x} \in \mathbb{R}^{\mathbf{n} \times \mathbf{n}},$$

with elements coming from (3.13). The stiffness term can be treated similarly. With the tensor gradient we can write it as a tensor K

$$(4.2) \quad K = \int_{\hat{\Omega}} [Q \cdot (\nabla \otimes B)] \cdot (\nabla \otimes B) \, d\hat{x} \in \mathbb{R}^{\mathbf{n} \times \mathbf{n}}.$$

$$(4.3) \quad = \sum_{k,l=1}^D \int_{\hat{\Omega}} q_{k,l} \frac{\partial}{\partial \hat{x}_l} B \otimes \frac{\partial}{\partial \hat{x}_k} B \, d\hat{x}$$

whose elements are of the form in (3.16). The associated mass and stiffness matrices are obtained by reordering the indices since the elements of the mass and stiffness tensors match the elements of the matrices.

Except for the D-variate weight functions ω and Q , the entries of the mass and stiffness tensors (4.1) and (4.2) are the product of univariate B-splines. The scalar $\omega(\hat{x}) = |\det \nabla G(\hat{x})|$ and the matrix $Q(\hat{x}) = (\nabla G(\hat{x})^{-1})(\nabla G(\hat{x}))^{-T} \omega(t) \in \mathbb{R}^{D \times D}$ are determined by the geometry mapping. As Mantzaflaris et al. suggest in [22], we can approximate these weight functions via interpolation by some combination of univariate functions,

$$(4.4) \quad \omega(\hat{x}) \approx \omega_1(\hat{x}^{(1)}) \cdots \omega_D(\hat{x}^{(D)}).$$

The integrands then are separable into products of univariate integrals. To further reduce the computation time and storage requirements of the mass and stiffness matrix calculation, the resulting interpolating function is approximated with low rank methods giving low rank approximations of the system matrices [21, 22].

To do so, we interpolate the weight functions by a combination of univariate B-splines of higher order, denoted by the spline space $\tilde{\mathbb{S}}^D$ with suitable knot vectors $\tilde{\xi}_d$ and degrees \tilde{p}_d with $d = 1, \dots, D$. The weight function $\omega(\hat{x})$ of the mass matrix is interpolated as

$$(4.5) \quad \omega(\hat{x}) \approx \sum_{\mathbf{j} \in \mathcal{J}} W_{\mathbf{j}} \tilde{\beta}_{\mathbf{j}}(\hat{x}) = W : \tilde{B}(\hat{x}),$$

where $\tilde{\beta}_{\mathbf{j}}(\hat{x})$ are the elements of the spline space $\tilde{\mathbb{S}}^D$ and $\tilde{B}(\hat{x})$ is the tensor holding all $\beta_{\mathbf{j}}$ ordered according to the index set \mathcal{J} . The weight tensor W has the same dimension as the

spline space $\tilde{\mathbb{S}}^D$, being $(\tilde{n}_1, \dots, \tilde{n}_D)$, and we get its entries by interpolating the weight function in a sufficient number of points, namely $\tilde{n} = \tilde{n}_1 \cdots \tilde{n}_D$.

We construct canonical low rank representations of the weight tensor,

$$(4.6) \quad W \approx \sum_{r=1}^R \bigotimes_{d=1}^D w_r^{(d)} =: W_R,$$

with $w_r^{(d)} \in \mathbb{R}^{n_d}$ to get a low rank representation of the weight function,

$$(4.7) \quad \omega(\hat{x}) \approx W_R : \tilde{B}(\hat{x}) = \sum_{r=1}^R \prod_{d=1}^D w_r^{(d)} \cdot \tilde{B}^{(d)}(\hat{x}^{(d)}).$$

Here $\tilde{B}^{(d)}(\hat{x}^{(d)}) \in \mathbb{R}^{n_d}$ denotes the vector holding all univariate basis functions evaluated in $\hat{x}^{(d)}$ as in (3.5), and “ \cdot ” is the scalar product. The entries of the mass matrix can be approximated using this low rank representation and we can calculate each entry as the sum of products of univariate integrals,

$$(4.8) \quad M_{\mathbf{i},\mathbf{j}} = \sum_{r=1}^R \prod_{d=1}^D \int_0^1 \beta_{i_d}^{(d)} \beta_{j_d}^{(d)} w_r^{(d)} \cdot \tilde{\beta}^{(d)} \, d\hat{x}^{(d)}.$$

With these univariate integrals we define a univariate mass matrix, which depends on some weight function ω , as

$$(4.9) \quad M^{(d)}(\omega) = \int_0^1 B^{(d)} \otimes B^{(d)} \omega \, d\hat{x}^{(d)},$$

where $B^{(d)} \in \mathbb{R}^{n_d}$ is the vector holding all n_d univariate B-splines of $\mathbb{S}_{\xi_d}^{p_d}$. According to the tensor representation in Equation (4.1), we can finally write the mass matrix as a sum of Kronecker products of small univariate mass matrices (4.9) with $\omega = w_r^{(d)} \cdot \tilde{\beta}^{(d)}$,

$$(4.10) \quad M = \sum_{r=1}^R \bigotimes_{d=1}^D M^{(d)}(w_r^{(d)} \cdot \tilde{\beta}^{(d)}).$$

The same procedure can be applied to the weight function of the stiffness matrix $Q(\hat{x})$. Note that $Q(\hat{x}) \in \mathbb{R}^{D \times D}$, thus we have to apply the interpolation to each entry of Q . Similarly to (4.7), for each entry of Q we get the canonical low rank representation

$$(4.11) \quad q_{k,l}(\hat{x}) \approx V_{k,l,R} : \tilde{B}(\hat{x}) = \sum_{r=1}^R \prod_{d=1}^D v_{k,l,r}^{(d)} \cdot \tilde{\beta}^{(d)}(\hat{x}^{(d)}), \quad \text{for all } k, l = 1, \dots, D,$$

with $v_{k,l,r}^{(d)} \in \mathbb{R}^{n_d}$.

Using this low rank method, we approximate the entries of the stiffness matrix as

$$(4.12) \quad K_{\mathbf{i},\mathbf{j}} = \sum_{k,l=1}^D \int_{\hat{\Omega}} \left(\prod_{d=1}^D \delta(l,d) \beta_{i_d}^{(d)} \delta(k,d) \beta_{j_d}^{(d)} \right) \sum_{r=1}^R \prod_{d=1}^D v_{k,l,r}^{(d)} \cdot \tilde{\beta}^{(d)} \, d\hat{x},$$

$$(4.13) \quad = \sum_{k,l=1}^D \sum_{r=1}^R \prod_{d=1}^D \int_0^1 \delta(l,d) \beta_{i_d}^{(d)} \delta(k,d) \beta_{j_d}^{(d)} v_{k,l,r}^{(d)} \cdot \tilde{\beta}^{(d)} \, d\hat{x}^{(d)},$$

where $\mathbf{j} = (j_1, \dots, j_D)$, and $\delta(k, d)$ denotes the operator acting on f as

$$(4.14) \quad \delta(k, d)f = \begin{cases} \frac{\partial f}{\partial \hat{x}_d} & \text{if } k = d, \\ f & \text{otherwise.} \end{cases}$$

To get a representation for the stiffness matrix corresponding to the mass matrix representation in (4.10), we define the D^2 univariate stiffness matrices dependent on some weight function $q^{(d)}(\hat{x}^{(d)})$ as

$$(4.15) \quad K_{k,l}^{(d)}(q^{(d)}) = \int_0^1 (\delta(l, d)B) \otimes (\delta(k, d)B) q^{(d)} d\hat{x}^{(d)}, \quad \text{for } k, l = 1, \dots, D.$$

With this and $q^{(d)} = v_{k,l,r}^{(d)} \cdot \tilde{\beta}^{(d)}$ the final low rank tensor representation of the stiffness matrix is

$$(4.16) \quad K = \sum_{k,l=1}^D \sum_{r=1}^R \bigotimes_{d=1}^D K_{k,l}^{(d)}(v_{k,l,r}^{(d)} \cdot \tilde{\beta}^{(d)}).$$

Strategies to efficiently compute the low rank representation for W have been discussed in [21] for two dimensional settings and for three dimensional settings with partial decompositions in [28] and using tensor decompositions in [28, 2].

We follow the strategy presented in [2] using low rank Tensor Train methods [24, 8] for the decompositions and further computations as it allows us to exploit the resulting low-rank structure.

5. The Alternating Minimal Energy solver for Tensor Train. The IAS algorithm requires solving the minimization problem (2.11) multiple times in line 4 of Algorithms 2.1 and 2.2. To solve the KKT system (3.28) we use a Block-structured Alternating Minimal Energy solver (AMEn) as proposed in [2]. The saddle point system is large and each block has a Kronecker product based structure. This structure can be interpreted as a low-rank Tensor-Train (TT) [24] representation. Alternatively, using a CGLS method with the reduced formulation (2.12) requires a large number of matrix-vector products with the matrix A . This matrix is dense and quickly gets unfeasibly large. Therefore, we want to avoid its complete computation and instead solve the matrix-vector product without explicitly forming A . We propose using the TT AMEn method to apply this computation as well.

The TT format is especially convenient for our purpose as the underlying Kronecker product structure of the parameter-to-observable map (3.23) – (3.25) can be interpreted as a low-rank Tensor-Train representation. Using the TT format we can easily compute the desired result in a low-rank format without exceeding the memory limitations of a standard computer even for large models, which usually are infeasible.

The Tensor-Train format represents a d -dimensional tensor $\mathbf{T} \in \mathbb{W}_{n_1, n_2, \dots, n_d}$ of order (n_1, n_2, \dots, n_d) with so-called TT-cores $T^{(k)} \in \mathbb{R}^{r_{k-1} \times n_k \times r_k}$ with TT-ranks r_k for $k = 1, \dots, d$. By convention we set $r_0 = r_d = 1$. Each TT-core can be interpreted as a parameter-dependent matrix $T^{(i)}(j_k) \in \mathbb{R}^{r_{k-1} \times r_k}$, $j_k = 1, \dots, n_i$ and every element of \mathbf{T} is represented as the product

$$(5.1) \quad \mathbf{T}(j_1, \dots, j_d) = T^{(1)}(j_1) \cdots T^{(d)}(j_d).$$

The whole tensor can be written as a sum of Kronecker products,

$$(5.2) \quad \mathbf{T} = \sum_{\alpha_1=1}^{r_1} \cdots \sum_{\alpha_d=1}^{r_d} \bigotimes_{k=1}^d \mathbf{T}_{\alpha_{k-1}, \alpha_k}^{(k)} =: tt(T^{(1)}, \dots, T^{(d)}),$$

where the subscripts α_{k-1}, α_k are row and column indices of the TT-core $T^{(k)}$. This format directly corresponds to the matrices in (3.23) – (3.25).

We want to solve an equation system $\mathbf{Ax} = b$ in this format, where \mathbf{A} is a tensor of size $N \times N$ with $N = (n_1, \dots, n_d)$ and \mathbf{x} and b are tensors of size N . This can be done efficiently with an energy function minimization cycling over the TT-cores, the *alternating linear scheme* (ALS) [16]. This approach constructs low-dimensional systems of linear equations for each core, which can then be solved with standard numerical methods. Here, we derive the method for symmetric \mathbf{A} . Solving $\mathbf{Ax} = b$ then corresponds to the minimization of the energy function,

$$(5.3) \quad \min_{\mathbf{x}} J(\mathbf{x}) = \|\mathbf{x}_* - \mathbf{x}\|_{\mathbf{A}}^2 = (\mathbf{x}, \mathbf{Ax}) - 2(\mathbf{x}, \mathbf{b}) + \text{const},$$

with the exact solution $\mathbf{x}_* = \mathbf{A}^{-1}\mathbf{b}$. To find a solution for (5.3) we make an initial guess \mathbf{x}_0 and cycle over its TT-cores where we solve a local problem to improve the current guess. For this, in iteration k all cores but the k -th are *frozen* and we minimize over

$$(5.4) \quad \mathbf{x}_{\text{new}} = tt\left(x^{(1)}, \dots, x^{(k-1)}, x_{\text{new}}^{(k)}, x^{(k+1)}, \dots, x^{(d)}\right)$$

$$(5.5) \quad x_{\text{new}}^{(k)} = \min_{x^{(k)}} J(\mathbf{x}_{\text{new}}).$$

The energy function $J(\mathbf{x})$ does not grow during updates and the solution will subsequently converge to a local minimum. The tensor-train format is linear in its cores, as

$$(5.6) \quad \mathbf{x} = tt\left(x^{(1)}, \dots, x^{(k)}, \dots, x^{(d)}\right) = \mathbf{x}_{\neq k} x_k,$$

where $\mathbf{x}_{\neq k}$ is the Tensor-Train where the k -th core $\mathbf{x}^{(k)} \in \mathbb{R}r_{k-1} \times n_k \times r_k$ is replaced by an identity operator of the same size and x_k is a vectorization of $x^{(k)}$. With this, the energy function for the local problem becomes

$$(5.7) \quad J(\mathbf{x}) = (\mathbf{Ax}_{\neq k} x_k, \mathbf{x}_{\neq k} x_k) - 2(\mathbf{b}, \mathbf{x}_{\neq k} x_k) = (\mathbf{x}_{\neq k}^* \mathbf{Ax}_{\neq k} x_k, x_k) - 2(\mathbf{x}_{\neq k}^* \mathbf{b}, x_k).$$

The gradient of (5.7) with respect to x_k is zero when

$$(5.8) \quad (\mathbf{x}_{\neq k}^* \mathbf{Ax}_{\neq k}) x_k = \mathbf{x}_{\neq k}^* \mathbf{b}.$$

Therefore, the solution to the local minimization is equal to a solution in a reduced basis. This problem is small and can be solved by standard numerical methods. For the general ALS approach the resulting TT-ranks - and therefore the maximum accuracy - are fixed by the ranks set in the initial guess. But with some extension we can adapt the TT-ranks of the solution dynamically. For the purpose of calculating a low-rank approximation, we chose the so-called *Alternating Minimal Energy* (AMEn) method [8].

Algorithm 5.1 Low-rank AMEn

-
- 1: Input: Initial guess \mathbf{x} with TT-ranks $r = (r_1, \dots, r_d)$, tolerance ϵ_0 and/or rank bounds r_{\max} , system in TT-format \mathbf{A}, \mathbf{b}
 - 2: **while** $\|\mathbf{Ax} - \mathbf{b}\| > \epsilon_0$ and $k < \text{maxIter}$ **do**
 - 3: Form $A_1 = \mathbf{x}_{\neq 1}^* \mathbf{A} x_{\neq 1}, b_1 = \mathbf{x}_{\neq 1}^* \mathbf{b}$
 - 4: Solve $A_1 u^{(1)} = b_1$
 - 5: Optional: Do an SVD-based compression of $u^{(1)}$
 - 6: Let $\mathbf{u} = \text{tt}(u^{(1)}, x^{(2)}, \dots, x^{(d)})$ and $\mathbf{r} = \mathbf{Au} - \mathbf{b}$
 - 7: **if** $\|\mathbf{r}\| < \epsilon_0$ **then**
 - 8: **return** $\mathbf{x} = \mathbf{u}$
 - 9: **end if**
 - 10: Find smallest-rank residual approximation $\bar{\mathbf{r}}$ with $\|\bar{\mathbf{r}} - \mathbf{r}\| \leq \epsilon_0 \|\mathbf{r}\|$ and/or $\text{rank}(\bar{\mathbf{r}}^{(1)}) \leq r_{\max}$
 - 11: Expand basis by first TT-core $\bar{r}^{(1)}$ of $\bar{\mathbf{r}}, x^{(1)} = \begin{bmatrix} u^{(1)} & \bar{r}^{(1)} \end{bmatrix}$, and accordingly $x^{(2)} = \begin{bmatrix} x^{(2)} \\ 0 \end{bmatrix}$
 - 12: Form $X_1 = x^{(1)} \otimes I_{n_2, \dots, n_d}$ of size $(n_1, \dots, n_d) \times (r_1 n_2, \dots, n_d)$
 - 13: Form the $(d-1)$ -dimensional system $A_{\geq 2} x_{\geq 2} = b_{\geq 2}$ with $A_{\geq 2} = X_1^* \mathbf{A} X_1, b_{\geq 2} = X_1^* \mathbf{b}$.
 - 14: **if** $d = 2$ **then**
 - 15: Solve $A_{\geq 2} x_{\geq 2} = b_{\geq 2}$ directly
 - 16: **else**
 - 17: Call AMEn recursively with $\mathbf{x} \leftarrow \text{tt}(x^{(2)}, \dots, x^{(d)}), \mathbf{A} \leftarrow A_{\geq 2}, \mathbf{b} \leftarrow b_{\geq 2}$.
 - 18: **end if**
 - 19: **end while**
 - 20: Output: low-rank solution $\mathbf{x} = \text{tt}(x^{(1)}, \dots, x^{(d)})$
-

The algorithm is outlined in [Algorithm 5.1](#). This method first solves a local system as in (5.8). Then it expands the components of the solution subsequently by local gradient information as in line 11 of the algorithm. Afterwards, the system dimension is reduced by one and the previous computation repeated in a recursive way until a 2D matrix equation system is reached. Solving this equation system finalizes the outer iteration after which all steps are repeated until reaching the convergence tolerance. The method proved to be robust and has a fast convergence rate. For a detailed analysis and more information we refer the reader to [8].

Using the TT notation and the AMEn method, we can compute matrix-vector products with A efficiently without forming the full matrix and get the resulting solution vectors in a low-rank format. For solving the block system (3.28) we use a block solver based on AMEn *AMEn Block Solve*, which exploits the block structure of (3.28) as well as the low rank tensor product structure of each component.

6. Numerical experiments. We want to illustrate the performance of our method with some numerical examples and analyze the choice of parameters for PDE problems. We first

r	η	β	ϑ
1	10^{-5}	$3/2 + \eta$	3.3
0.5	10^{-3}	$(3/2 + \eta)/r$	8.3
-1	$\beta + 3/2$	3	1.5×10^{-4}

Table 1: Parameters for the three hyper models

present results for different parameter settings for a two dimensional domain and later show results for a 3D model. The parameters for the different hypermodel setups are listed in [Table 1](#).

Example 1: 2D domain. First, let us consider a two dimensional domain with sparse heat sources, as shown in [Figure 2a](#). This domain is discretized using IGA with 32 B-splines per dimension resulting in 1024 spatial degrees of freedom. The total rank for the mass matrix is 8 and for the stiffness matrix we have a combined number of 12 low-rank components. For the time discretization we use $N_t = 50$.

This setup is governed by a heat distribution

$$(6.1) \quad \frac{\partial x}{\partial t}(t) = 0.1\Delta x(t) \quad \text{in } \Omega \times (0, 1]$$

$$(6.2) \quad x(0) = x_0 \quad \text{in } \Omega \times (t = 0)$$

$$(6.3) \quad x(t) = 0 \quad \text{on } \partial\Omega \times [0, 1]$$

and we measure the state only once after 50 time steps at $T = 1$. The resulting state is shown in [Figure 2b](#) and is measured under noise $e \sim \mathcal{N}(0, 0.1)$. We run a non-modified IAS algorithm with hyperprior parameters as in the first row of [Table 1](#) with $r = 1$, as suggested in [4]. We do 50 IAS steps and 30 CGLS steps per iteration. For the low-rank matrix vector products we set a tolerance of 10^{-6} . The solver tolerance for AMEn was set to 10^{-4} and we do a maximum of 20 AMEn steps per iteration. An exemplary result is shown in [Figure 2c](#). We see that the solution indeed fits the very sparse initial state perfectly. The algorithm successfully reconstructs the 4 sources. For comparison the result for a least squares reconstruction is shown in [Figure 2d](#).

Example 2: Hyperprior parameters. Let us now take a closer look at the parameters of the generalized gamma distribution used for the hyperprior in [Equation \(2.5\)](#) and the performance of the local and global hybrid IAS algorithm. We use the same setup as before. We set up a globally convex hyperprior model with $r = 1$ two different sparsity inducing models with $r = 0.5$ and $r = -1$ to compare the performance of the different algorithm variations. The rest of the parameters correspond to [Table 1](#).

We will compare three different methods: CGLS with a full computation of A denoted by full CGLS that will not be feasible for large scale problems; CGLS with low-rank matrix-vector products in TT format denoted by TT CGLS; and solving the KKT system of the constrained optimization problem with the block AMEn method denoted by AMEn.

First, let us review the global hybrid IAS switching models after 10 iterations. In [Figure 3](#) we see results for the two different hypermodel setups with $r = -1$ and $r = 0.5$. We compare

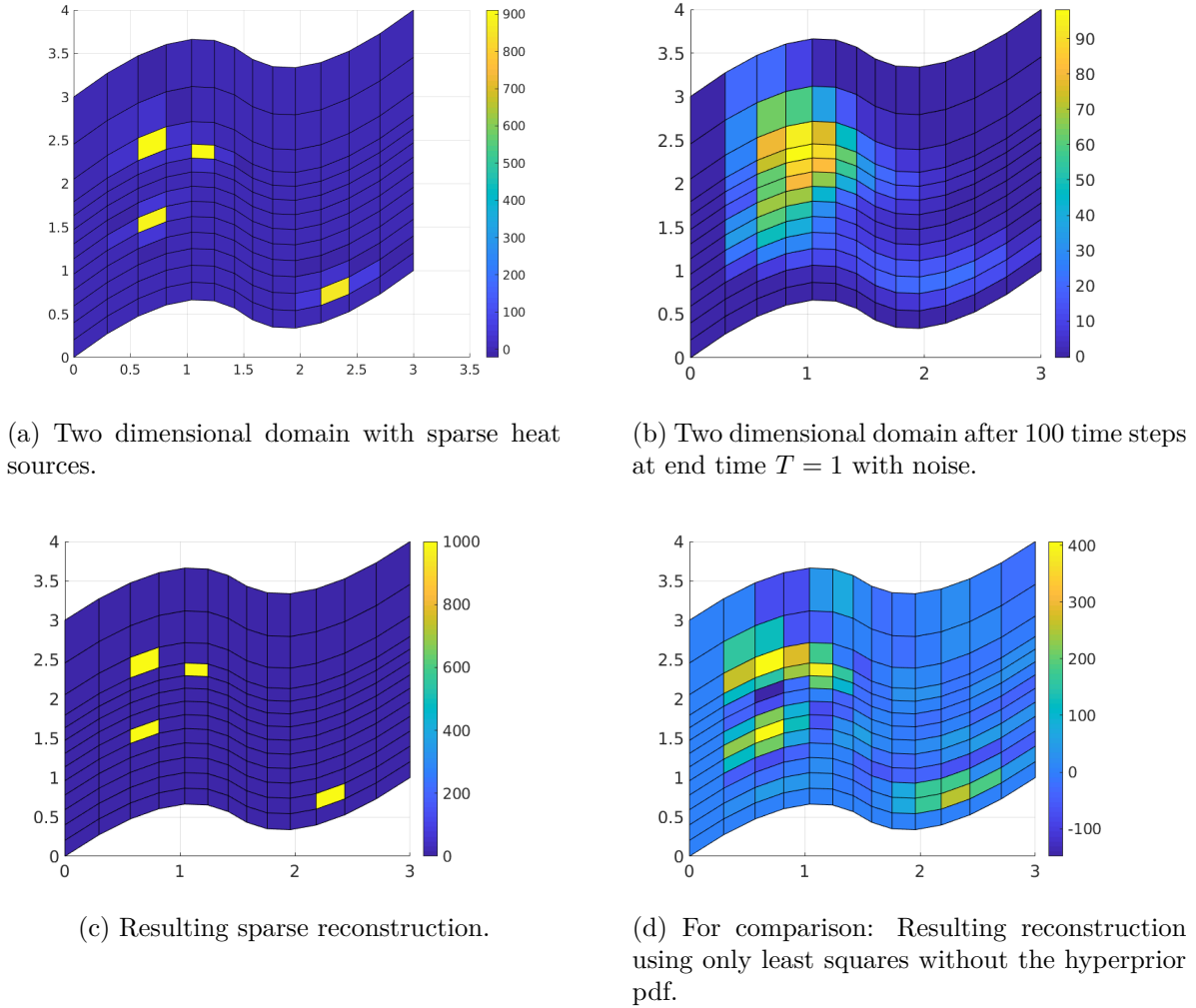
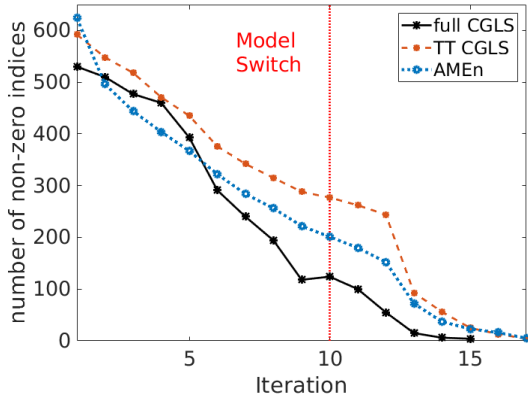
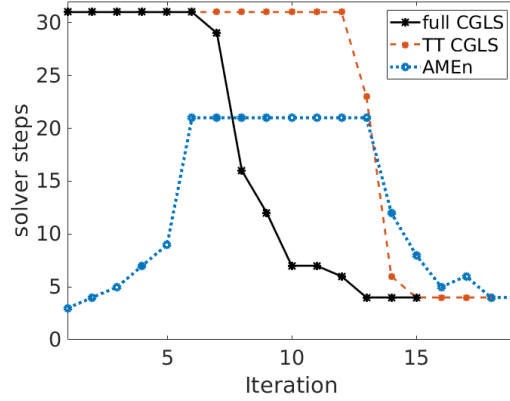


Figure 2: Setup for the 2D example problem. The PDE is discretized using 1024 basis functions.

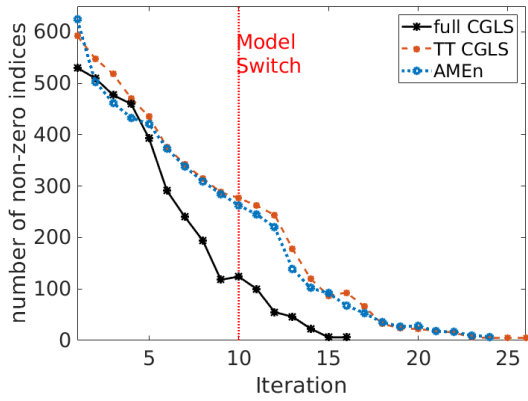
the performance of the low-rank CGLS and the constrained optimization with AMEn. Both setups start out with a globally convex hypermodel with $r = 1$. After 10 iterations the first algorithm switches to a greedy hypermodel with $r = -1$, indicated by a red vertical line. We can see the number of non-zero entries reducing shortly after the tenth iteration in Figure 3a for $r = -1$. In Figure 3b, we see that the CGLS method starts with the maximum number of iterations and the low-rank version requires more IAS steps until the number of local iterations starts reducing compared to the full CGLS method. This can be attributed to the inexact matrix-vector products leading to inexact descent directions. Nonetheless, the low-rank CGLS converges with only a small number of extra iterations required.



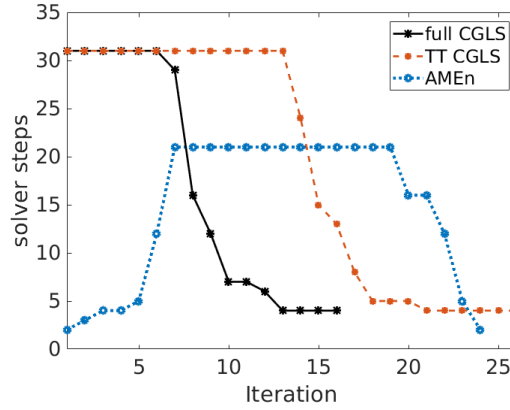
(a) Number of indices for which u_0 is non-zero per iteration for $r = -1$. The switch to the model with stronger sparsity promotion is indicated by the red dotted line.



(b) CGLS steps and AMEn sweeps per iteration for the global hybrid IAS with $r = -1$.



(c) Number of indices for which u_0 is non-zero per iteration for $r = 0.5$. The switch to the model with stronger sparsity promotion is indicated by the red dotted line.



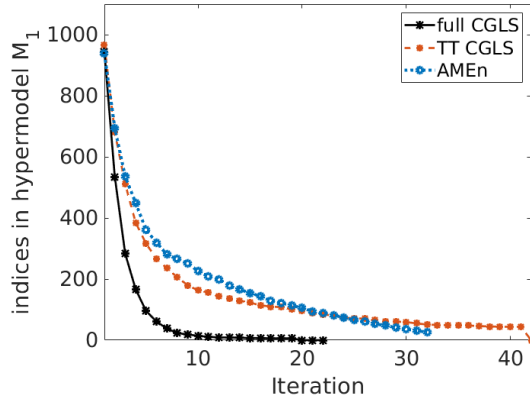
(d) CGLS steps and AMEn sweeps per iteration for the global hybrid IAS with $r = 0.5$.

Figure 3: Development of non-zero indices and CGLS steps for the global hybrid IAS. We compare using the full matrix A with CGLS (full CGLS), CGLS with low-rank matrix-vector products (TT CGLS) and a constrained minimization with AMEn.

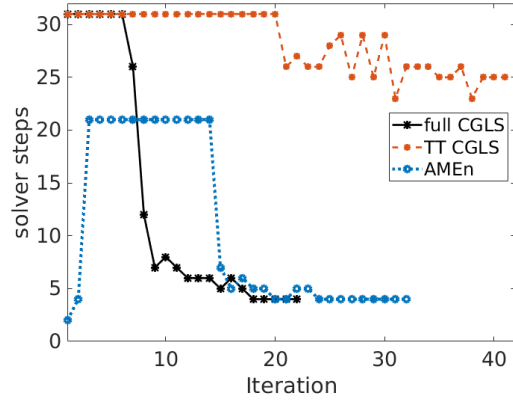
The constrained optimization method does not require the full number of 20 steps from the beginning. This is due to $D_\theta^{-1/2}$ starting out quite large. This could be interpreted as a large regularization parameter for u_0 in the optimization, which is generally easier to solve. As θ changes, the minimization gets more challenging before the iteration numbers

start decreasing again. All three algorithms converge with the local solvers needing 4 steps for their last iterations, which corresponds to the number of non-zero values in u_0 .

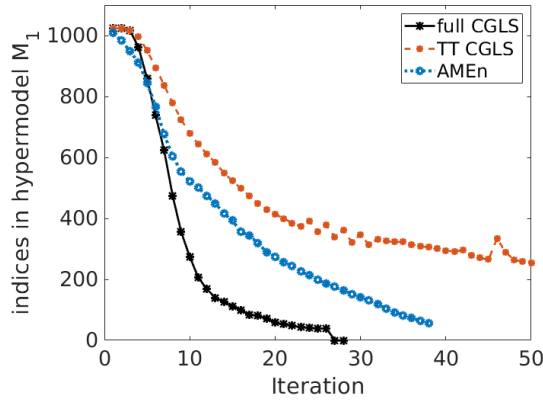
In Figures 3c and 3d we see very similar results for a second model with $r = 0.5$. Note, that both algorithms are equal until iteration 10 where we switch to the different second models. For $r = 0.5$ convergence is not reached as fast as for $r = -1$, which was to be expected as $r = -1$ promotes sparsity more strongly. Again we see a quick reduction in non-zero entries shortly after the switch to the second hyper model in Figure 3c. And as before the low-rank methods need some more iterations to converge, as seen in Figure 3d.



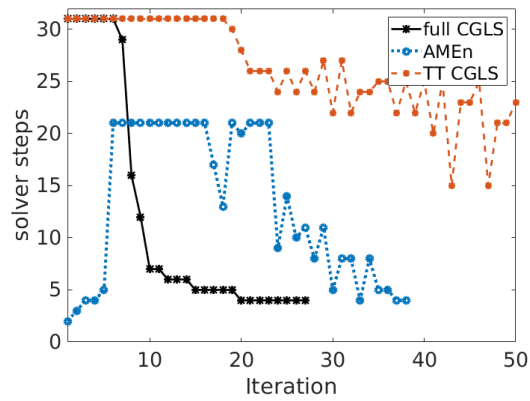
(a) Number of indices remaining in hypermodel M_1 in each iteration for the local hybrid IAS with inverse gamma $r = -1$.



(b) CGLS and AMEn steps per iteration for the local hybrid IAS with $r = -1$.



(c) Number of indices remaining in hypermodel M_1 in each iteration for the local hybrid IAS with less greedy gamma parameter $r = 0.5$.



(d) CGLS and AMEn steps per iteration for the local hybrid IAS with $r = 0.5$. CGLS with TT did not reach convergence.

Figure 4: We compare using the full matrix A with CGLS (full CGLS), CGLS with low-rank matrix-vector products (TT CGLS) and a constrained minimization with AMEn.

		global		local	
		iterations	residual	iterations	residual
full CGLS	$r = -1$	15	2.3e-7	22	9.8e-3
	$r = 0.5$	16	5.9e-6	28	7.2e-3
TT CGLS	$r = -1$	18	9.2e-7	41	4.8e-2
	$r = 0.5$	26	2.6e-6	> 50	0.4
AMEn	$r = -1$	18	3.6e-4	32	8.3e-2
	$r = 0.5$	24	2.4e-4	38	8.2e-2

Table 2: Number of total iterations and residual error to the original initial state as $\|u_0 - u\|/\|u_0\|$ with true initial state u_0 and reconstruction u .

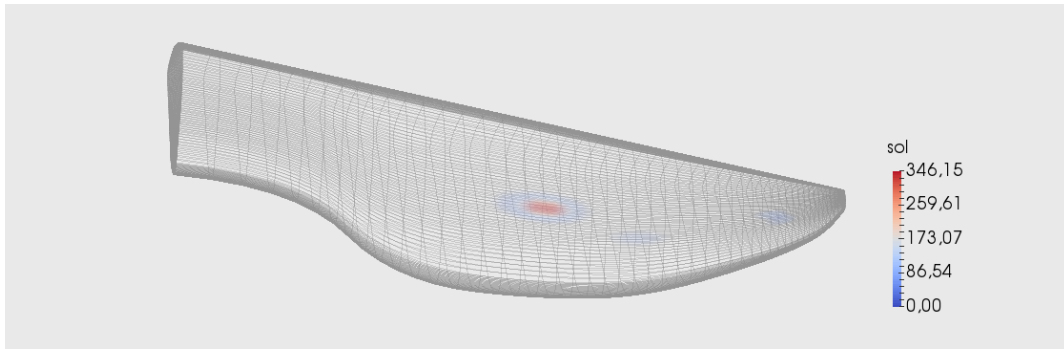
Next, we look at the local hybrid IAS. Here, the switch to the second models is done individually for each entry of θ as described in [subsection 2.1](#). The results are shown in [Figure 4](#). The first row shows the performance with $r = -1$ for the second model. In [Figure 4a](#) we see the number of entries in θ , which remain in the first hypermodel with $r = 1$. All others are switched to $r = -1$ as soon as their convexity condition is fulfilled. We see that the constrained minimization with AMEn performs quite well. The number of parameters remaining in the model with $r = 1$ is reducing quickly. The low-rank CGLS requires some more iterations but ultimately converges as well. In [Figure 4b](#), we see that again the AMEn method ends up converging with only 4 local iterations towards the end of the algorithm, similar to the full CGLS method. The low-rank TT CGLS however requires a large number of steps until the very end when it converges.

Additionally, in [Figures 4c](#) and [4d](#) we see the results for a model with $r = 0.5$. As expected the method needs more iterations to converge and the number of indices in θ remaining in the first model decreases more slowly for all three algorithms in [Figure 4c](#). Again, the full CGLS and AMEn converge with 4 local iterations towards the last iterations of the algorithms. However, the TT CGLS does not converge within 50 outer iterations. Here, a smaller residual tolerance for the matrix-vector products might result in more successful steps.

The number of iterations and the resulting residual with respect to the actual initial state are listed in [Table 2](#). We see that overall the results for the global method are very good. The larger residuals for AMEn correspond to the solver tolerance, which was set at 10^{-4} . For the local method however all methods required a larger number of iterations and the resulting reconstruction was not as close to the original as for the global method.

Example 2: 3D domain. We now consider a three dimensional domain with a more complex geometric model. The low-rank structure has a much higher rank than the previous example, namely 10 factors for the mass and 180 factors for the stiffness matrix. The initial state is displayed in [Figure 5a](#) and the final state we use for the reconstruction with noise $\sigma = 0.1$ in [Figure 5b](#). An exemplary reconstruction with global hybrid IAS and $r_2 = -1$ is displayed in [Figure 6](#).

We modify the problem size by changing the space discretization size and number of time steps to observe the scaling behavior of the method. For the TT CGLS method we set the



(a) Three dimensional domain with sparse heat sources.

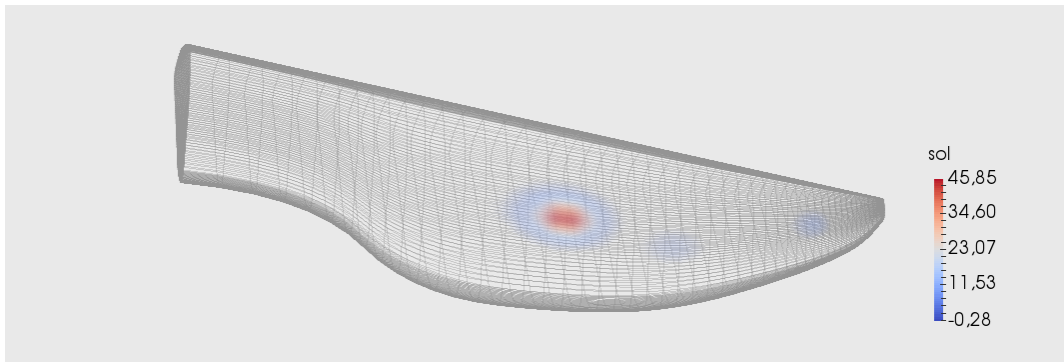
(b) Three dimensional domain after 100 time steps at end time $T = 1$ with noise.

Figure 5: Setup for the 3D example problem

tolerance to $1e-6$. The result for two spatial discretizations and three different time resolutions is displayed in [Table 3a](#). The setups with equal spatial discretization behave very similarly. For a total of 756 degrees of freedom all time discretizations result in less than 10 iterations. For the discretization with 6048 spatial nodes some more iterations are required but again the method displays similar behavior for all time discretizations. For the constrained minimization with AMEn the behavior is quite different. Here, we display three spatial discretizations and two time discretizations in [Table 3](#). For the different spatial resolutions the number of IAS iterations is somewhat stable. But with a larger number of time steps the required iterations increase drastically. In future research, we aim to mitigate this behavior by further tailoring the AMEn solver regarding the enrichment process and the design of suitable preconditioners.

7. Outlook. We demonstrated that combining low rank tensor methods with sparsity inducing hyperprior models gives us a powerful method for the reconstruction of sparse initial states for large scale PDE systems. We tested different parameter setups for the local and global version of the hybrid IAS algorithm and compared the performance of different local solvers. The IAS algorithm requires a number of subsequent solutions of a large scale minimization problem. We can solve the arising problems with standard methods for quadratic

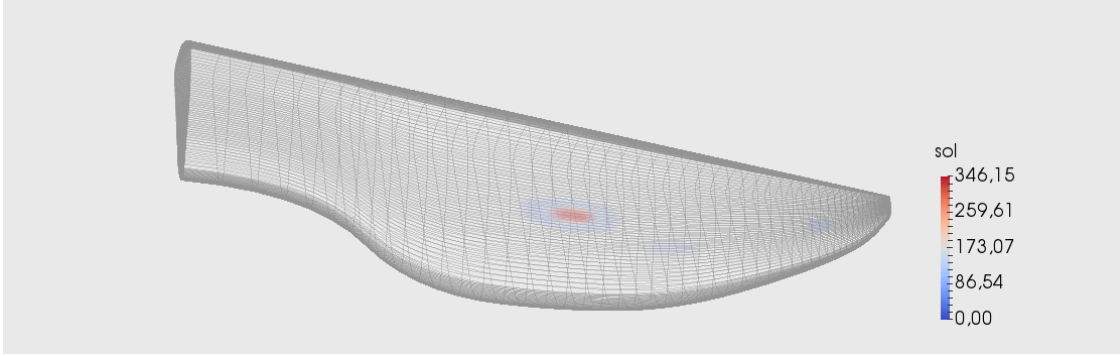
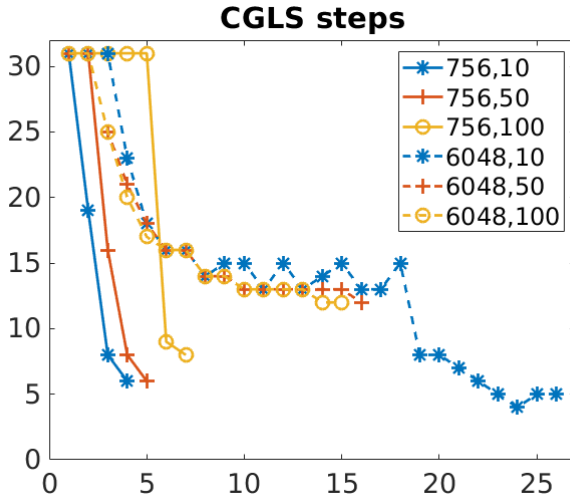


Figure 6: Resulting sparse reconstruction for the 3D example problem



$N_t \backslash n$	756	6048	48384
50	16	18	29
100	47	50	49

Table 3: Number of IAS steps using a constrained minimization formulation with AMEn for the global hybrid IAS with $r = -1$ and the 3D model problem for different levels of discretization.

(a) Number of IAS steps for the global hybrid IAS with $r = -1$ and the 3D model problem for different discretization sizes. Here we used TT CGLS

minimization like CLGS or formulate a constrained optimization problem. In the context of IGA discretization, both representations can be solved efficiently using tensor train calculations and the Alternating Minimal Energy solver (AMEn) designed to work with low rank Kronecker product based problems.

In combination with an Isogeometric space discretization, tensor train calculations can be very efficient. In future research, we want to enhance the methods performance by equipping it with suitable preconditioning and a more fitting local solver. This will allow us to solve sparse reconstruction problems for large-scale three dimensional discretizations.

Acknowledgements. The authors would like to thank Daniela Calvetti for her helpful insights and sharing of implementations.

The work of the authors was supported by the German Science Foundation (DFG) through grant 1742243256 - TRR 9.

REFERENCES

- [1] Z. BOFANG, *The Finite Element Method*, John Wiley & Sons Singapore Pte. Ltd, Apr. 2018.
- [2] A. BÜNGER, S. DOLGOV, AND M. STOLL, *A low-rank tensor method for PDE-constrained optimization with isogeometric analysis*, SIAM J. Sci. Comput., 42 (2020), pp. A140–A161.
- [3] D. CALVETTI, M. PRAGLIOLA, AND E. SOMERSALO, *Sparsity promoting hybrid solvers for hierarchical Bayesian inverse problems*, SIAM J. Sci. Comput., 42 (2020), pp. A3761–A3784.
- [4] D. CALVETTI, M. PRAGLIOLA, E. SOMERSALO, AND A. STRANG, *Sparse reconstructions from few noisy data: Analysis of hierarchical Bayesian models with generalized gamma hyperpriors*, Inverse Probl., 36 (2020), p. 025010.
- [5] D. CALVETTI, E. SOMERSALO, AND A. STRANG, *Hierarchical Bayesian models and sparsity: ℓ_2 -magic*, Inverse Probl., 35 (2019), p. 035003.
- [6] E. J. CANDÉS, J. K. ROMBERG, AND T. TAO, *Stable signal recovery from incomplete and inaccurate measurements*, Comm. Pure Appl. Math., 59 (2006), pp. 1207–1223.
- [7] J. A. COTTRELL, T. J. HUGHES, AND Y. BAZILEVS, *Isogeometric Analysis*, John Wiley & Sons, Ltd, Aug. 2009.
- [8] S. V. DOLGOV AND D. V. SAVOSTYANOV, *Alternating minimal energy methods for linear systems in higher dimensions*, SIAM J. Sci. Comput., 36 (2014), pp. A2248–A2271.
- [9] D. L. DONOHO, *Superresolution via sparsity constraints*, SIAM J. Math. Anal., 23 (1992), pp. 1309–1331.
- [10] ———, *For most large underdetermined systems of linear equations the minimal ℓ_1 -norm solution is also the sparsest solution*, Comm. Pure Appl. Math., 59 (2006), pp. 797–829.
- [11] H. ELMAN, D. SILVESTER, AND A. WATHEN, *Finite Elements and Fast Iterative Solvers*, Numerical Mathematics and Scientific Computation, Oxford University Press, second ed., June 2014.
- [12] G. FARIN, *NURBS for Curve & Surface Design*, A K Peters/CRC Press, Mar. 1999.
- [13] M. GRASMAIR, M. HALTMEIER, AND O. SCHERZER, *Sparse regularization with ℓ_q penalty term*, Inverse Probl., 24 (2008), p. 055020.
- [14] M. HESTENES AND E. STIEFEL, *Methods of conjugate gradients for solving linear systems*, J. Res. Natl. Bur. Stan., 49 (1952), p. 409.
- [15] M. HINZE, *A variational discretization concept in control constrained optimization: The linear-quadratic case*, Comput Optim Applic, 30 (2005), pp. 45–61.
- [16] S. HOLTZ, T. ROHWEDDER, AND R. SCHNEIDER, *The alternating linear scheme for tensor optimization in the tensor train format*, SIAM J. Sci. Comput., 34 (2012), pp. A683–A713.
- [17] T. HUGHES, J. COTTRELL, AND Y. BAZILEVS, *Isogeometric analysis: CAD, finite elements, NURBS, exact geometry and mesh refinement*, Comput. Method. Appl. M., 194 (2005), pp. 4135–4195.
- [18] B. JIN, P. MAASS, AND O. SCHERZER, *Sparsity regularization in inverse problems*, Inverse Probl., 33 (2017), p. 060301.
- [19] M. JUNCOSA AND D. YOUNG, *On the Crank-Nicolson procedure for solving parabolic partial differential equations*, Math. Proc. Camb. Phil. Soc., 53 (1957), pp. 448–461.
- [20] B. KNAPIK, A. VAN DER VAART, AND J. VAN ZANTEN, *Bayesian recovery of the initial condition for the heat equation*, Communications in Statistics - Theory and Methods, 42 (2013), pp. 1294–1313.
- [21] A. MANTZAFLARIS, B. JÜTTLER, B. KHOROMSKIJ, AND U. LANGER, *Matrix generation in isogeometric analysis by low rank tensor approximation*, in Curves and Surfaces: 8th International Conference, Paris, France, June 12-18, 2014, Revised Selected Papers, Springer International Publishing, 2015, pp. 321–340.
- [22] A. MANTZAFLARIS, B. JÜTTLER, B. N. KHOROMSKIJ, AND U. LANGER, *Low rank tensor methods in Galerkin-based isogeometric analysis*, Comput. Method. Appl. M., 316 (2017), pp. 1062–1085.
- [23] H. MINGYOU AND V. THOMÉE, *On the backward Euler method for parabolic equations with rough initial data*, SIAM J. Numer. Anal., 19 (1982), pp. 599–603.
- [24] I. OSELEDETS, *Tensor-train decomposition*, SIAM J. Sci. Comput., 33 (2011), pp. 2295–2317.
- [25] J. W. PEARSON, M. STOLL, AND A. J. WATHEN, *Regularization-robust preconditioners for time-dependent*

- PDE-constrained optimization problems*, SIAM J. Matrix Anal. & Appl., 33 (2012), pp. 1126–1152.
- [26] L. PIEGL, *On NURBS: A survey*, IEEE Comput. Grap. Appl., 11 (1991), pp. 55–71.
- [27] S. RAO, *The Finite Element Method in Engineering*, Elsevier, sixth edition ed., 2018.
- [28] F. SCHOLZ, A. MANTZAFLARIS, AND B. JÜTTLER, *Partial tensor decomposition for decoupling isogeometric Galerkin discretizations*, Comput. Method. Appl. M., 336 (2018), pp. 485–506.
- [29] J. R. SHEWCHUK, *An introduction to the conjugate gradient method without the agonizing pain*, tech. rep., Carnegie Mellon University, USA, 1994.
- [30] M. STOLL AND T. BREITEN, *A low-rank in time approach to PDE-constrained optimization*, SIAM J. Sci. Comput., 37 (2015), pp. B1–B29.
- [31] S. SUBRAMANIAN, K. SCHEUFELE, M. MEHL, AND G. BIROS, *Where did the tumor start? an inverse solver with sparse localization for tumor growth models*, Inverse Probl., 36 (2020), p. 045006.
- [32] C. A. ZARZER, *On Tikhonov regularization with non-convex sparsity constraints*, Inverse Probl., 25 (2009), p. 025006.